Supplemental Figures

Supplemental Figure S1

A

Datasets generated in this study		Heart	Liver	Cerebellum	Olfactory bulb	Primary NSCs	Total	
ChIP-seq	Total H3	2,2,2 (6)	2,2,2 (6)	2,2,2 (6)	2,2,2 (6)	4,4,4 (12)	36	102
	H3K4me3	2,2,2 (6)	2,2,2 (6)	2,2,2 (6)	2,2,2 (6)	4,4,4 (12)	36	
	H3K27ac	2,2,2 (6)	2,2,2 (6)	2,2,2 (6)	2,2,2 (6)	2,2,2 (6)	30	
RNA-seq		3,3,3 (9)	3,3,3 (9)	3,3,3 (9)	3,2,3 (8)	2,2,2 (6)	41	

143 datasets

Young (3 months)
Middle-aged (12 months)
Old (29 months)

B Liver aging representative H&E histology

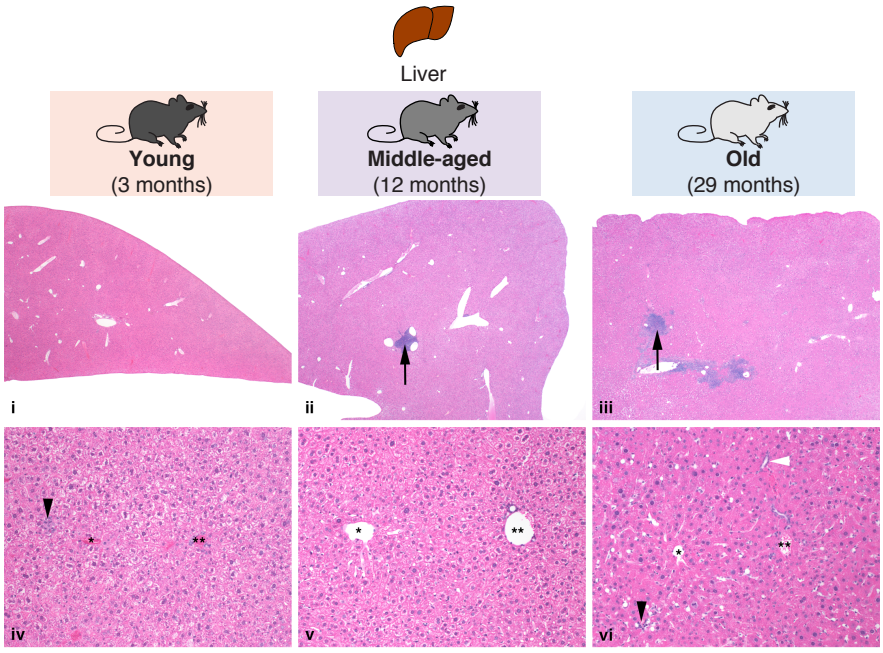

C Properties of primary NSCs cultures with increasing animal age

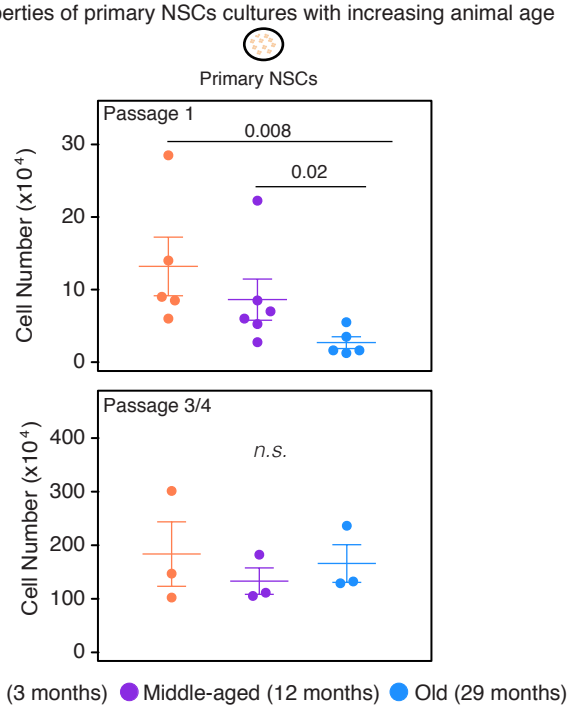

D MDS for H3K4me3 breadth (Top 5% broadest H3K4me3 domains)

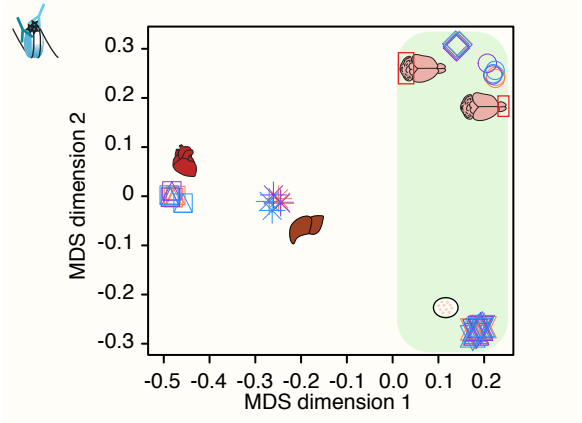

E MDS for H3K27ac intensity (Super-enhancers)

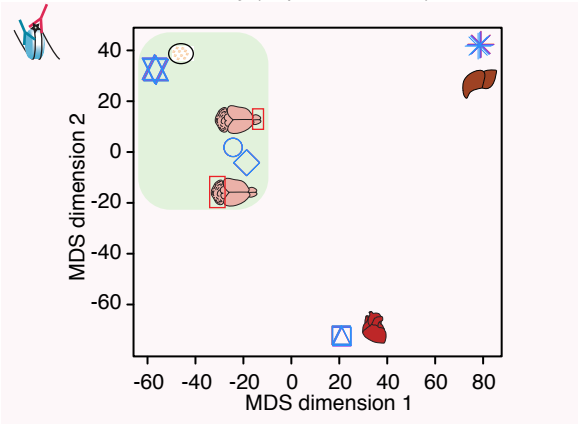

F PCA for for RNA expression

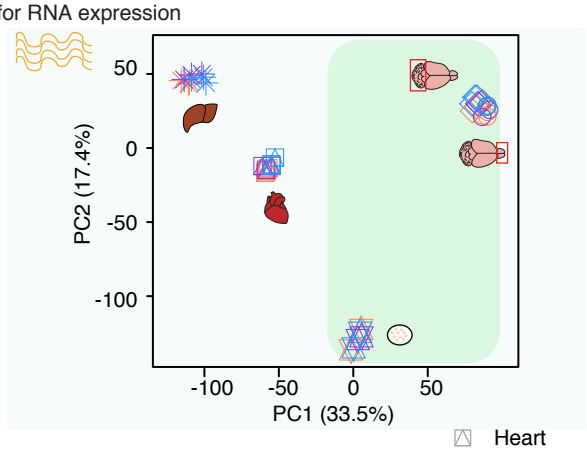

G PCA for for H3K4me3 breadth

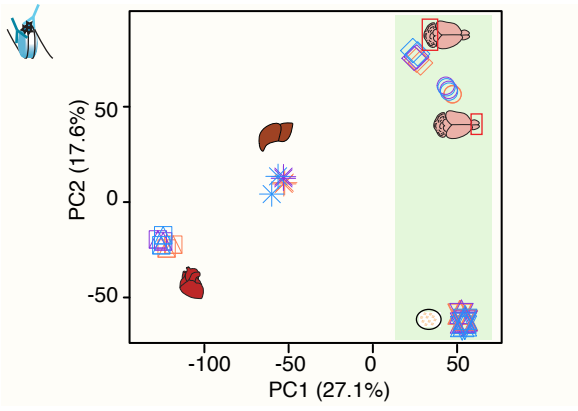

Heart
Liver
Neural lineage
Cerebellum
Olfactory bulb
Primary NSCs

Young (3 months)
Middle-aged (12 months)
Old (29 months)

Supplemental Figure S1. Mouse aging multi-omics dataset across 4 tissues and 1 cell type. (A) Summary of the datasets generated in this study. Also see **Supplemental Table S1A-D**. (B) Liver histology of 3 month (i, iv), 12 month (ii, v), and 29 month old (iii, vi) C57BL/6N mice paired to the RNA-seq cohort from this study. Tissue sections were stained with Hematoxylin and Eosin (H&E), and magnification is 2x (upper panels) and 40x (lower panels). With age, undulation of the hepatic capsule (iii) and perivascular lymphoid aggregates (ii, iii - black arrows) are evident compared to 3 month old mice (i). Mild (v) and moderate (vi) increase in cell (anisocytosis) and nuclear size (anisokaryosis) was present in old individuals compared to 3 month old mice (iv). Additional histologic findings at 29 months (vi) included bile duct hyperplasia (white arrowhead), extramedullary hematopoiesis (black arrowheads), increased sinusoidal cellularity, and increased numbers of lipid-laden Ito cells. Single and double asterisks denote central veins and portal triads, respectively. (C) Properties of primary NSCs cultures with increasing animal age at the end of passages 1 and 3/4. Mean +/- SEM of 5-6 independent primary NSCs cultures. Each dot corresponds to an independent NSC culture derived from an independent pool of 5 mice. P-values were calculated using a Mann-Whitney test. *n.s.* = not significant. (D-E) Multidimensional Scaling analysis results across datasets based on the breadth of the top 5% broadest H3K4me3 domains (D), or H3K27ac peak intensity at super-enhancers only (E). (F-G) Principal Component Analysis (PCA) results across datasets based on RNA expression (F), or H3K4me3 peak breadth (G) provided for comparison to MDS results. For RNA-seq data, the MDS and PCA input was a matrix of $\log_2$-transformed DESeq2 1.6.3 normalized counts. For chromatin marks, the most intense or broadest peak associated to a gene was used when more than one peak was present, and the $\log_2$-transformed normalized intensity or breadth was used as MDS and PCA input data (see Supplemental Material).

Supplemental Figure S2

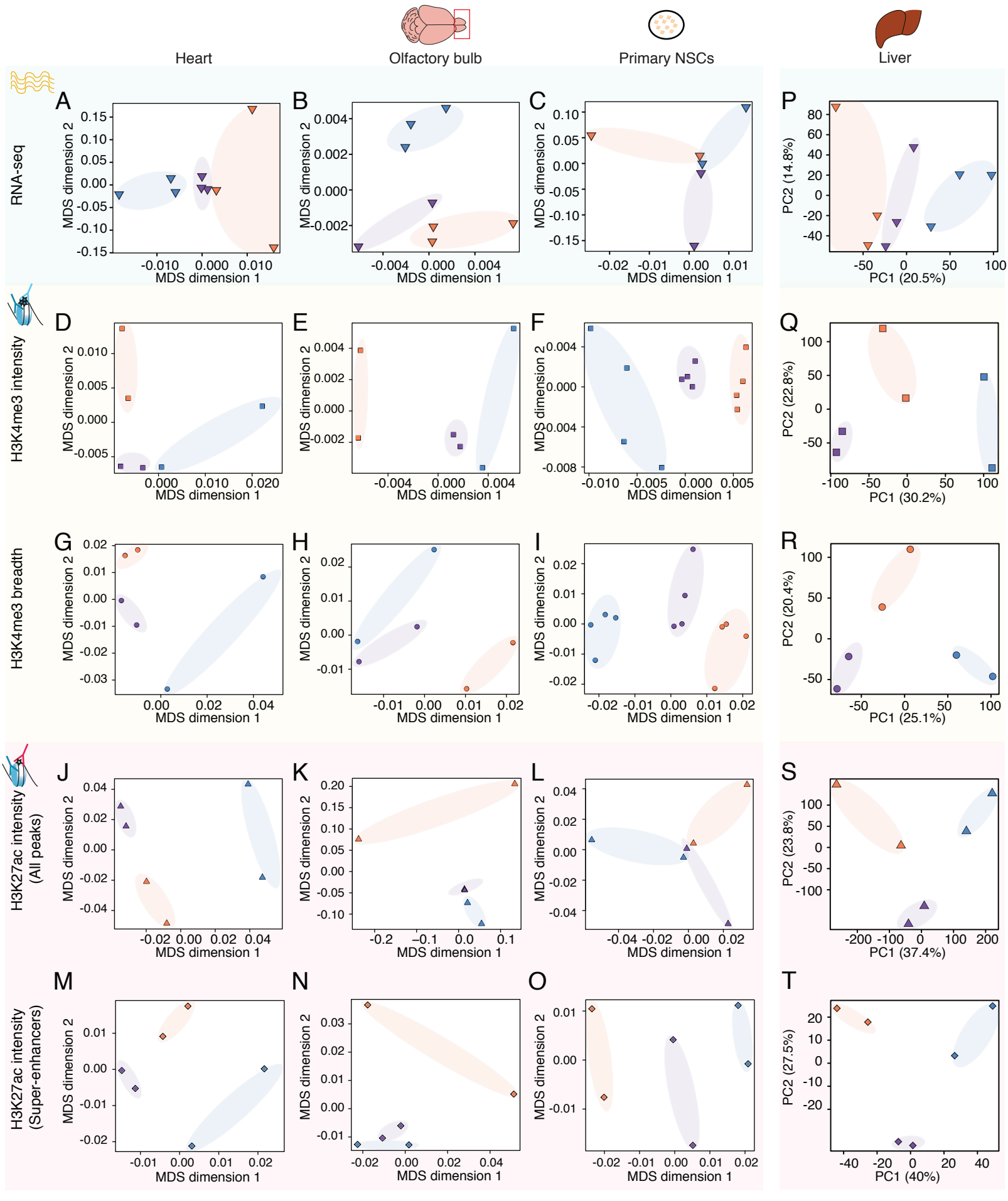

Supplemental Figure S2. Separation of samples across tissues and cell types as a function of age. Multidimensional Scaling (MDS) analysis results across samples derived from specific tissues, Heart, Olfactory Bulb and primary NSCs cultures, based on RNA expression (A-C), H3K4me3 intensity (D-F), H3K4me3 breadth (G-I), H3K27ac intensity (all peaks: J-L; super-enhancers only: M-O). Corresponding example of Principal Component Analysis (PCA) analysis results across liver samples (P-T). For RNA-seq data, the MDS and PCA input was a matrix of $\log_2$-transformed DESeq2 1.6.3 normalized counts. For chromatin marks, the most intense or broadest peak associated to a gene was used when more than one peak was present, and the $\log_2$-transformed normalized intensity or breadth was used as MDS and PCA input data (see Supplemental Material).

Supplemental Figure S3

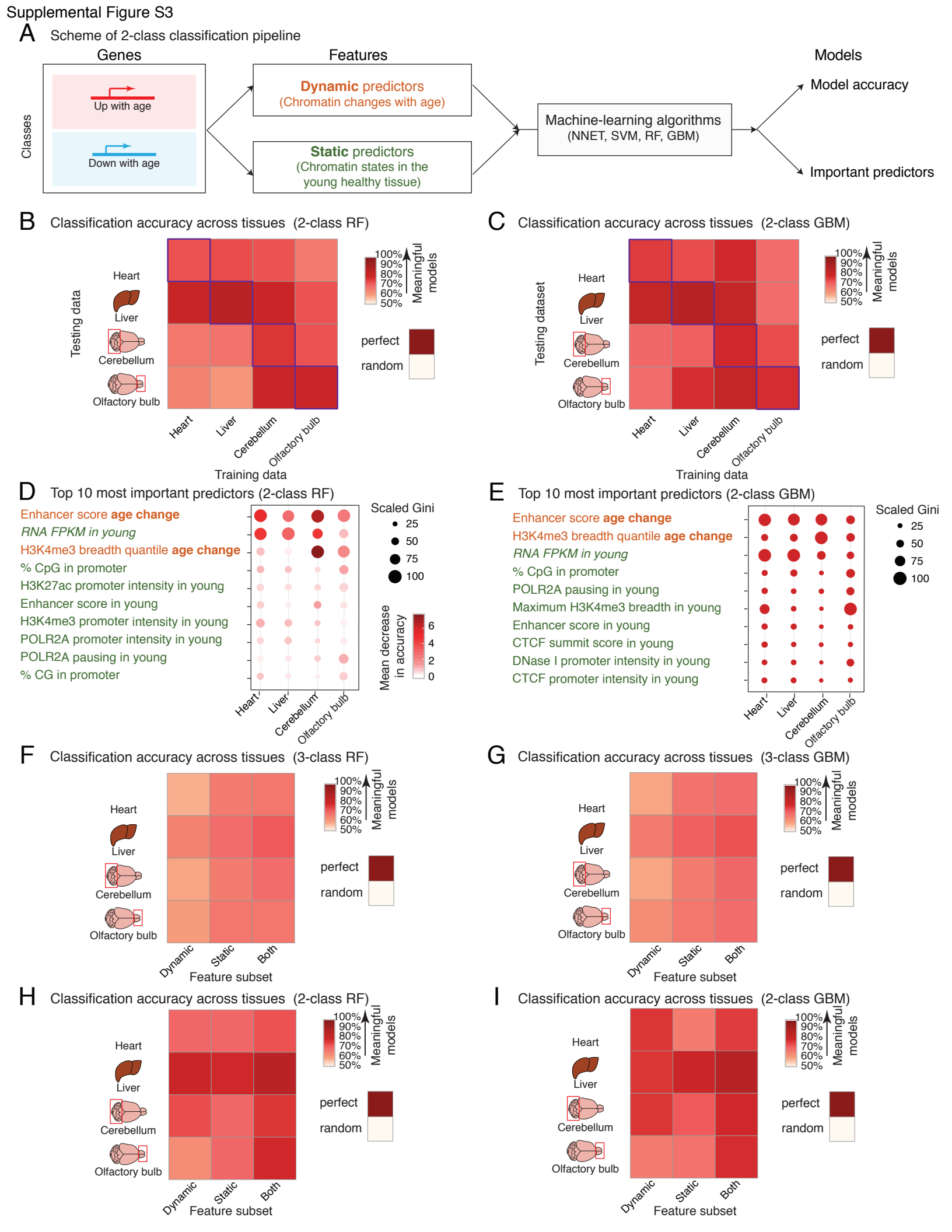

Supplemental Figure S3. Machine-learning analysis reveals that changes in enhancer score and H3K4me3 breadth with age can predict transcriptional aging (2-class classification).

(A) Scheme of the 2-class machine learning pipeline. NNET: neural network, SVM: support vector machine, RF: random forest, GBM: gradient boosting machine. (B-C) Classification accuracy over the 2-classes (*i.e.* upregulated vs. downregulated genes) cross tissues for Random Forest models (B) or Gradient Boosting Machine models (C). The accuracy of the model trained in a specific tissue on the same tissue (*e.g.* the liver-trained model on liver data) is measured using held-out validation data, and for cross-tissue validation, the entire data of the other tissue was used. 'Random' accuracy is displayed to illustrate the accuracy of a meaningless model (~50%). All tests were more accurate than random. (D-E) Feature importance from Random Forest models (D; Gini and mean decrease in accuracy) or Gradient Boosting Machine models (E; Gini). High values indicate important predictors. See analysis of 3-class models in **Fig. 3**. Note that 2-class models systematically outperformed 3-class models, which is consistent with the increased complexity of a classification problem with the number of classes to discriminate. (F-I) Classification accuracy over the 3- or 2-classes cross tissues for Random Forest models (F, H) or Gradient Boosting Machine models (G, I) with dynamic, static, or both dynamic and static features. The accuracy of the model trained in a specific tissue on the same tissue (*e.g.* the liver-trained model on liver data) is measured using held-out validation data. 'Random' accuracy is displayed to illustrate the accuracy of a meaningless model (~50%). All tests were more accurate than random.

Supplemental Figure S4

A Number of genes or loci with significant age-remodeling across cells and tissues (FDR<5%)

	RNAseq	H3K4me3 intensity	H3K4me3 breadth	H3K4me3 breadth (top 5%)	H3K27ac intensity (All peaks)	H3K27ac intensity (Super-enhancers)
Heart	203	104	426	36	447	39
Liver	409	534	754	58	4890	289
Cerebellum	735	629	261	17	6135	30
Olfactory bulb	198	74	217	15	71	0
Primary NSCs	0	12	268	11	9	0

B Example loci with H3K4me3 intensity remodeling with age (Liver)

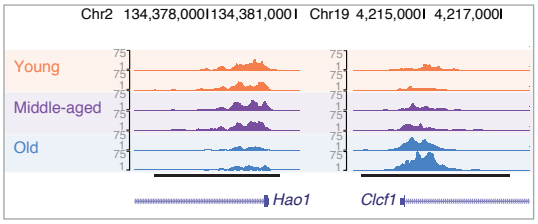

C Example loci with H3K4me3 breadth remodeling with age (Liver)

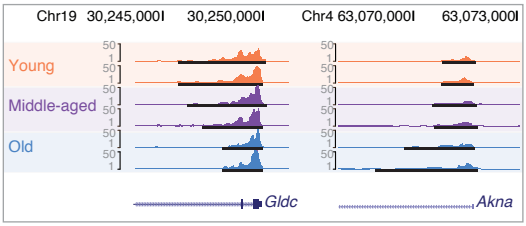

D Example loci with H3K27ac intensity (All peaks) remodeling with age (Liver)

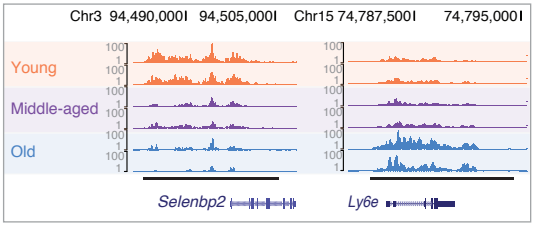

E Chromatin mark remodeling with aging (Liver and Cerebellum example)

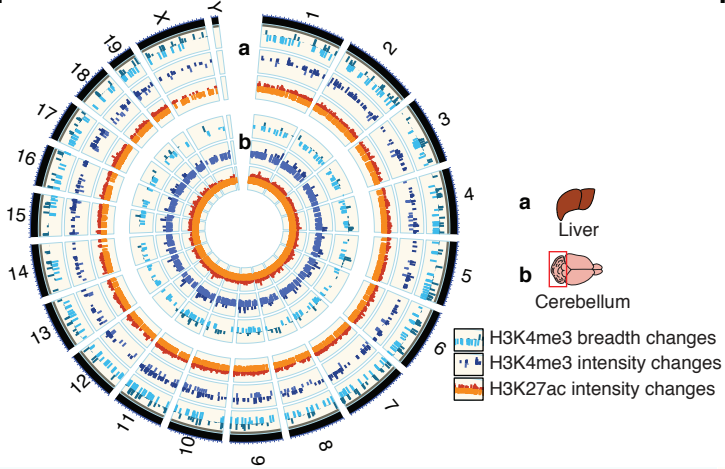

F Tissue-independent transcriptional changes with aging (FDR<5%)

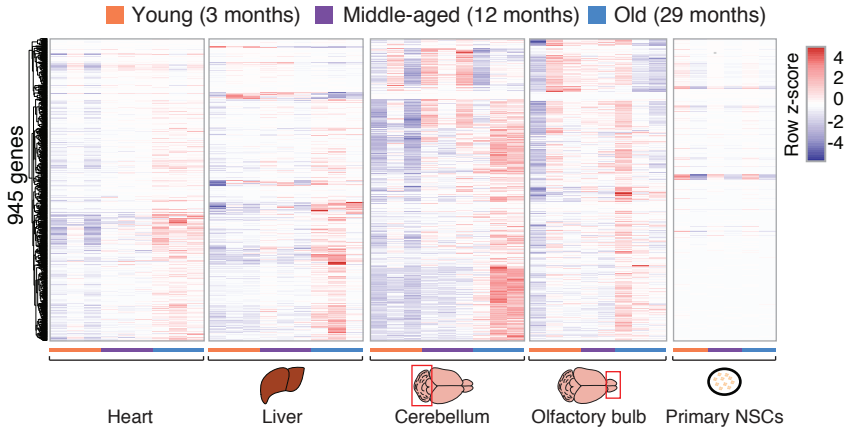

G Enrichments for differential RNA levels (KEGG 2017)

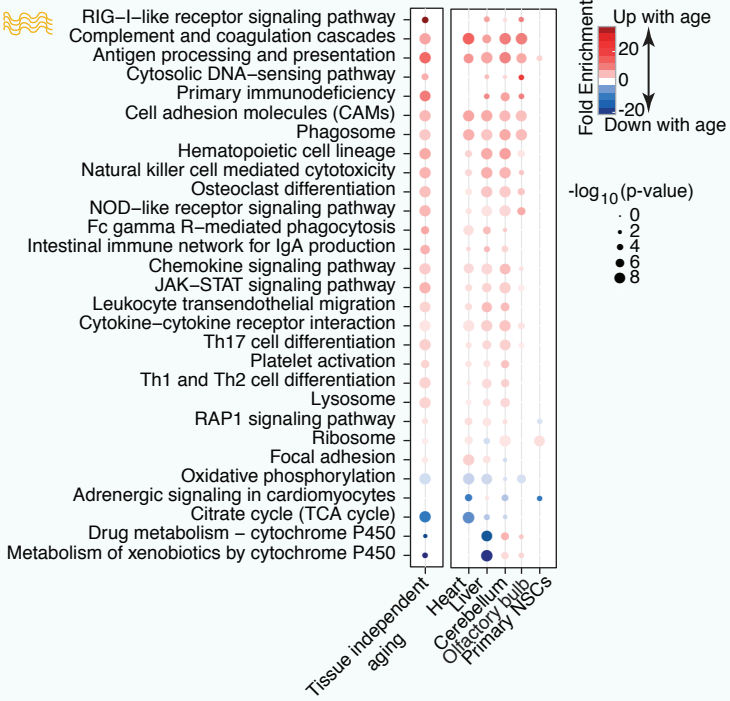

H Enrichments for differential H3K4me3 intensity (KEGG 2017)

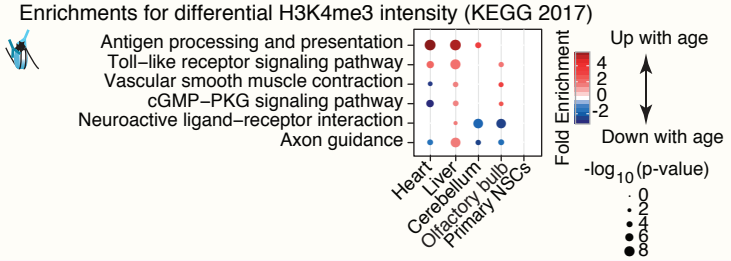

I Enrichments for differential H3K27ac intensity (KEGG 2017)

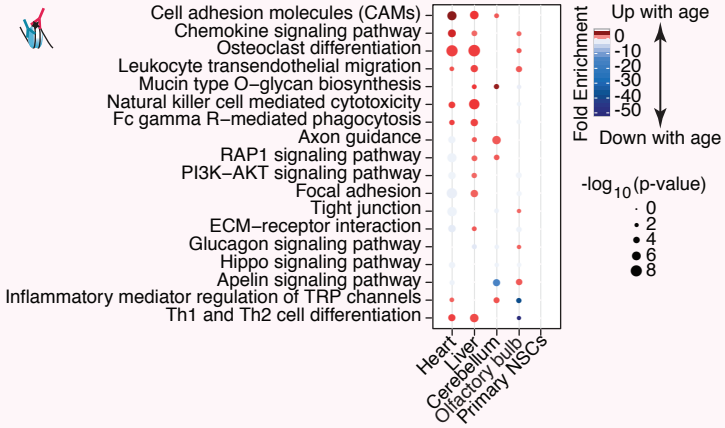

Supplemental Figure S4. Age-related transcriptomic and epigenomic remodeling.

(A) Table of the number of genes or loci with significant age-remodeling across cells and tissues (FDR<5%). (B-D) UCSC Genome Browser Shots for example of significantly remodeled loci in the liver samples. Chr: chromosome. (E) Circular genome plot showing the genomic distribution of regions with significantly remodeled H3K4me3 breadth, H3K4me3 intensity or H3K27ac intensity in Liver (a) or Cerebellum (b). Note that there is no obvious clustering on a specific chromosome. (F) Heatmap of genes with significant tissue-independent transcriptional changes with aging in each tissue and cells. Gene expression differences were called by DESeq2 1.6.3 with a significance threshold of FDR < 5%. Also see **Supplemental Table S4**. (G-I) Functional enrichments using the minimum hypergeometric (mHG) test at for differential RNA expression (C), differential H3K4me3 intensity (D), and differential H3K27ac intensity (all enhancers) (E). Note that none of the KEGG 2017 pathways were significantly enriched using genes with differential H3K4me3 breadth. Enriched pathways are plotted if 4 out of the 6 tests (RNA) or 3 out of the 5 tests (chromatin marks) were significant (FDR < 5%).

Supplemental Figure S5

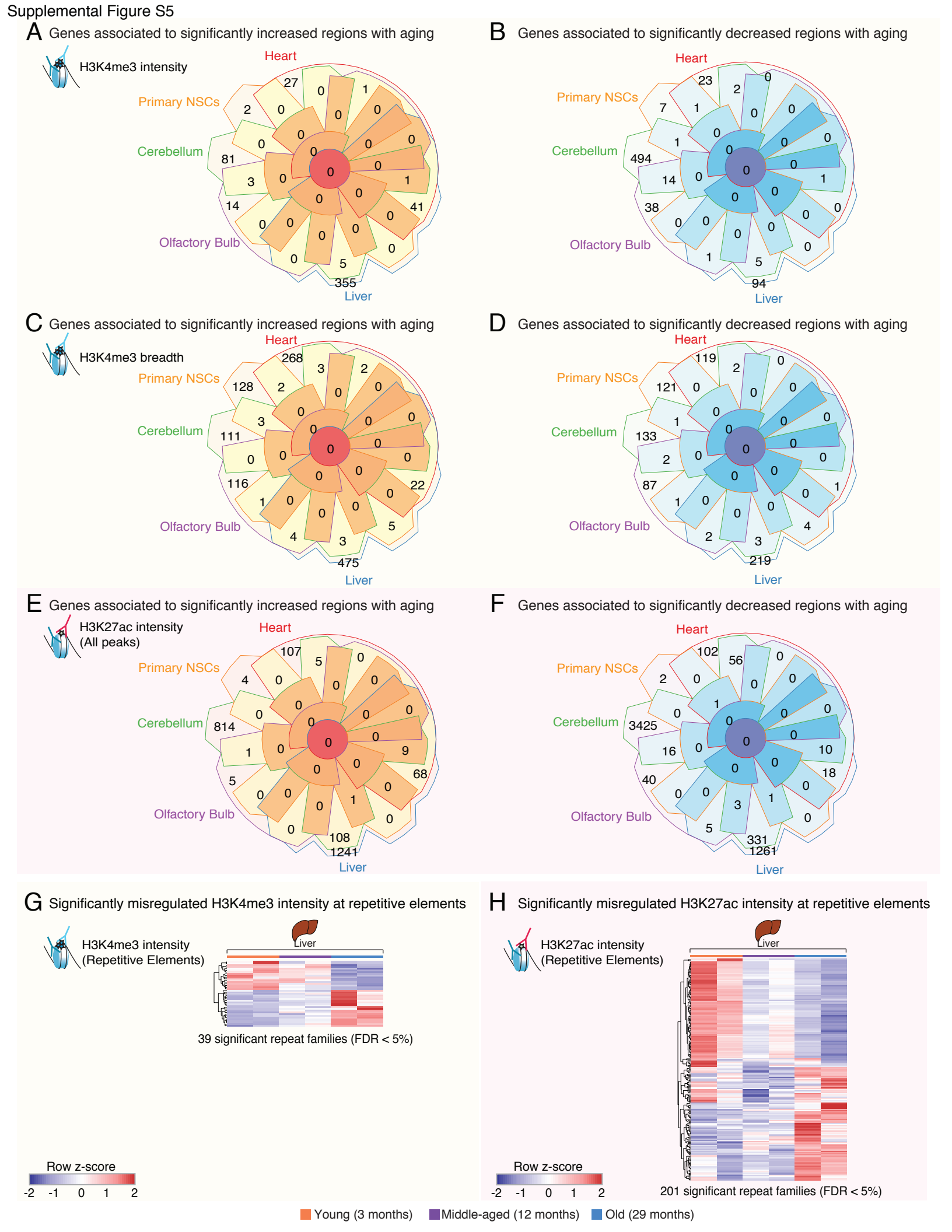

Supplemental Figure S5. Analysis of significantly remodeled chromatin domains with aging. (A-F) Overlap analysis for genes with (A,C,E) upregulated domains or (B,D,F) downregulated domains at FDR < 5% across tissues and cell types. Domains were associated to the closest transcriptional start site using HOMER (Heinz et al. 2010). Note that no gene was found to have recurrent significant chromatin remodeling across tissues. (G-H) Example heatmaps of H3K4me3 (G) or H3K27ac (H) intensity at significantly remodeled repeat families in the liver. Data from all tissues are reported in **Supplemental Table S6F-I**.

Supplemental Figure S6

RNA

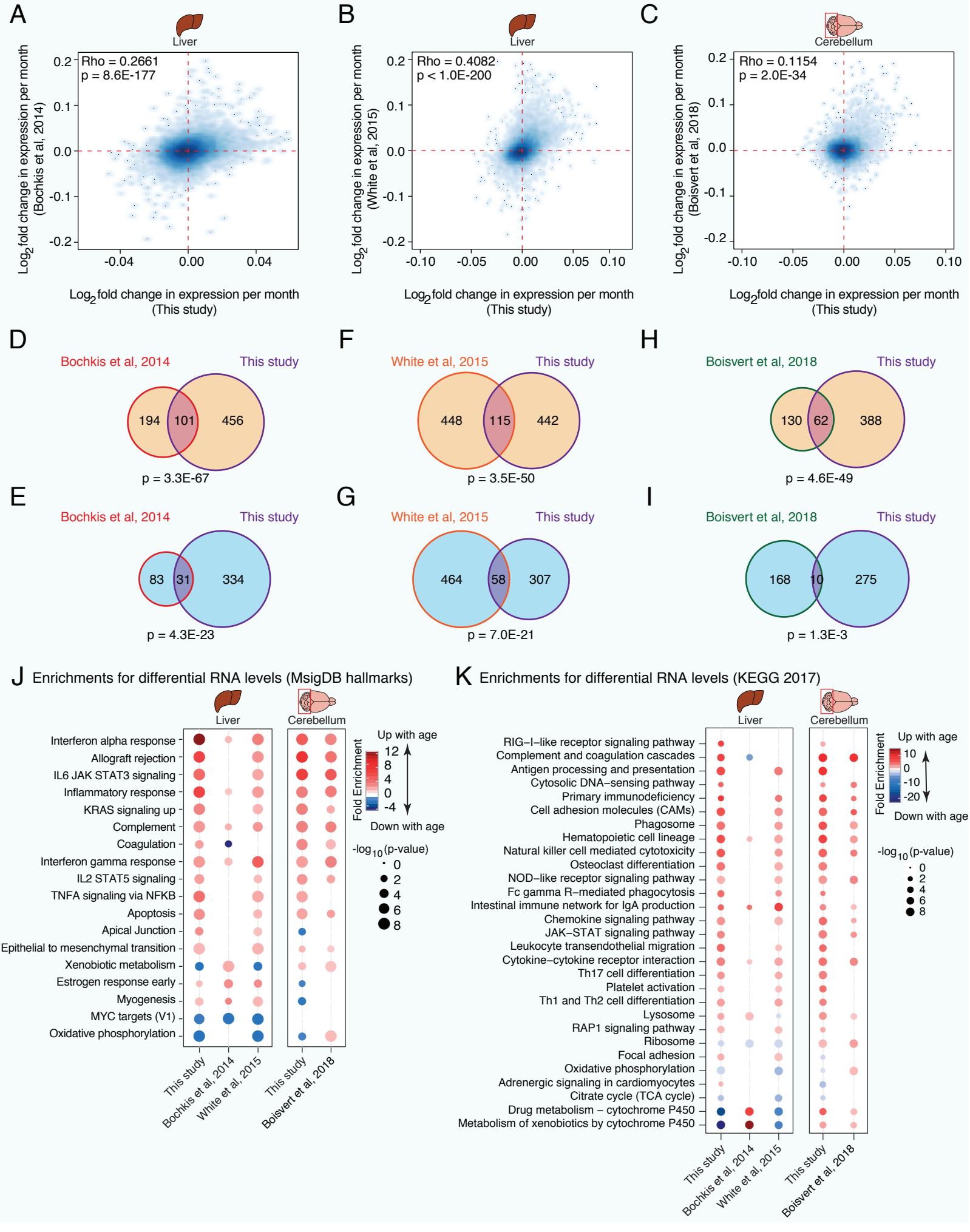

Supplemental Figure S6. Comparison of aging RNA-seq datasets in liver and cerebellum.
(A-C) Scatter plot of DESeq2 $\log_2$-fold change per month comparing liver (A-B) or cerebellum (C) transcriptomes to published RNA-seq datasets from liver (Bochkis et al. 2014; White et al. 2015) and cerebellum astrocytes (Boisvert et al. 2018). DESeq2 1.6.3 was used for our data, and DESeq2 1.16.1 for published datasets, as they were analyzed later in the course of the study [see methods]. Spearman's correlation (Rho) is reported for the fold change of gene expression in our dataset and the published datasets. The significance of the Rho value is also reported. (D-I) Venn diagrams of overlap for significantly regulated genes at FDR < 5% across listed datasets. Reported p-values were calculated using a one-sided Fisher's exact test. (J-K) Functional enrichments using the minimum hypergeometric (mHG) test for differential RNA expression with aging in our datasets and datasets from (Bochkis et al. 2014; White et al. 2015; Boisvert et al. 2018). For our liver and cerebellum datasets, the data are a subset of the panel shown in **Supplemental Fig. S4G** and are plotted as a reference point.

Supplemental Figure S7

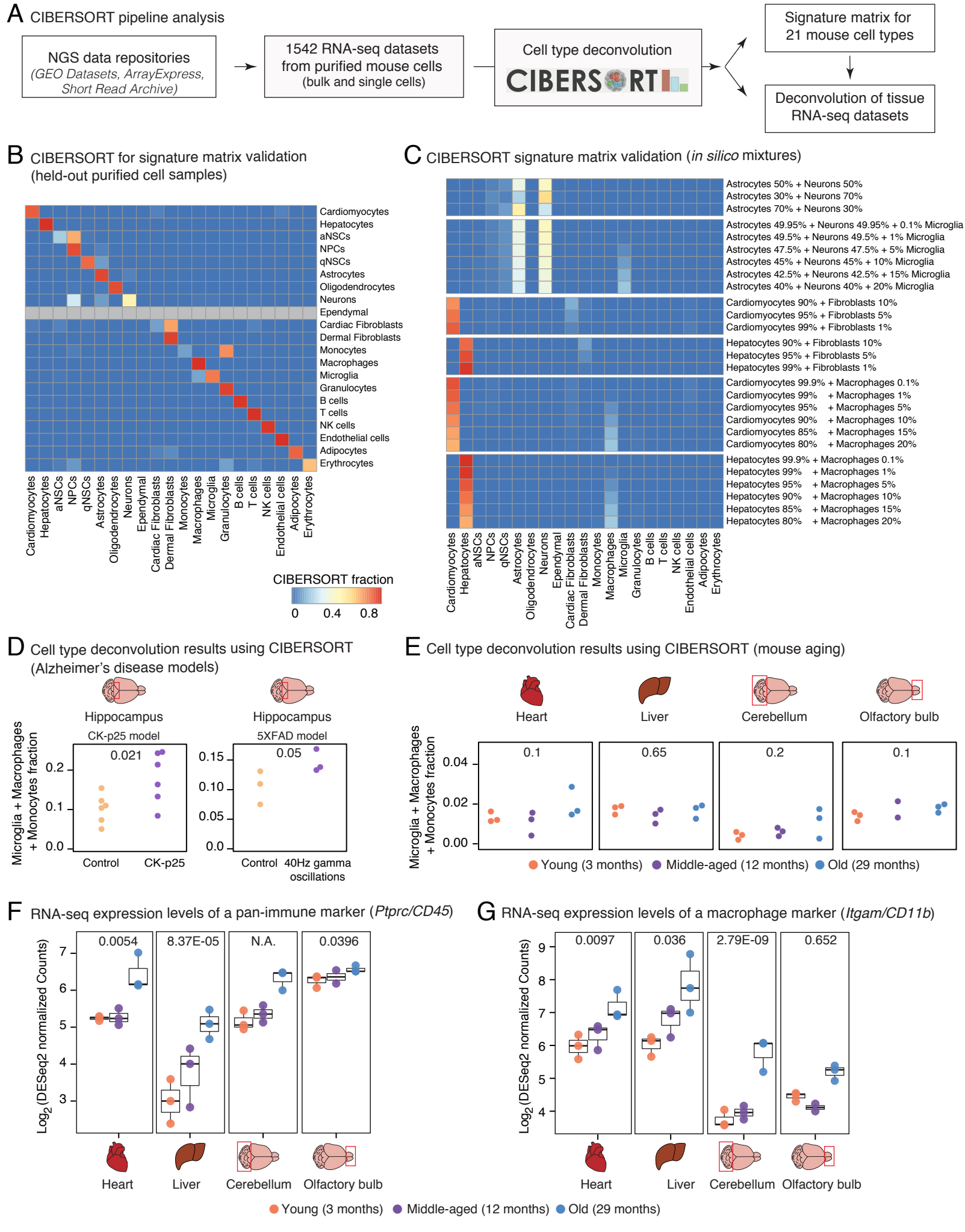

Supplemental Figure S7. CIBERSORT pipeline and signature matrix validation.

(A) Scheme of the CIBERSORT analysis pipeline. The signature matrix was built using publicly available RNA-seq datasets derived from pure cell types that are expected in the tissues analyzed (**Supplemental Table S2B**). (B) Heatmap of predicted cell type fractions on held-out purified RNA-seq samples using trained CIBERSORT Signature Matrix (see methods). aNSCs: activated Neural Stem Cells; qNSCs: quiescent Neural Stem Cells. (C) Heatmap of predicted cell type fractions on RNA-seq *in silico* mixtures of known cell types using trained CIBERSORT Signature Matrix (see Supplemental Material). aNSCs: activated Neural Stem Cells; qNSCs: quiescent Neural Stem Cells. (D) RNA deconvolution analysis of hippocampus RNA-seq datasets derived from mouse models with known increased inflammatory cell content (in particular microglia) and activity. (Left panel) CK-p25 Alzheimer's mouse model (Gjoneska et al. 2015); (Right panel) 5XFAD Alzheimer's mouse model following forced 40Hz gamma oscillations, reported to increase microglia number and activity (Iaccarino et al. 2016). P-values were calculated using a one-sided Wilcoxon test, to test for an increase in inflammatory cell content. Also see **Supplemental Table S7C**. (E) RNA deconvolution analysis of tissue aging RNA-seq datasets. P-values were calculated using a one-sided Wilcoxon test, to test for an increase in inflammatory cell content between the 3 month and 29 month samples. Linear regression tests as a function of age were also non-significant. Also see **Supplemental Table S7D**. (F-G) Boxplots of DESeq2 1.6.3 normalized counts (log_2 scale) for expression of immune marker genes *Ptrpc/CD45* and *Itgam/CD11b*. FDR from DESeq2 analyses of changes in aging gene expression are reported. N.A.: not calculated by DESeq2. For the boxplot representation: the thick bar is the sample median, the upper and lower edges of the box are the first and third quartiles of the data, and the whiskers are placed at 1.5 times the Inter Quartile range (IQR), as coded in the 'base' R package.

Supplemental Figure S8

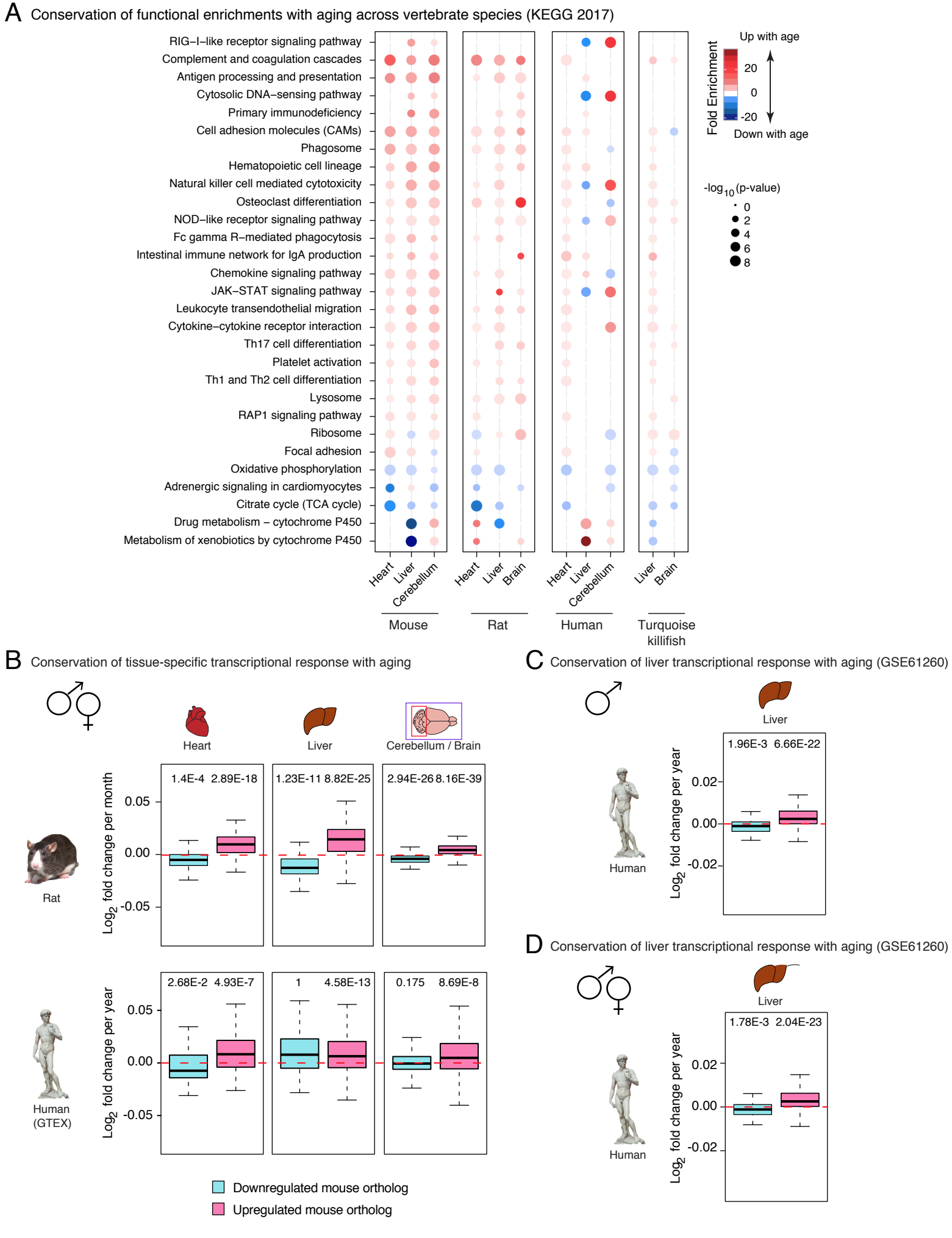

Supplemental Figure S8. Conservation of age-related transcriptional trajectories in vertebrate species.

(A) Functional enrichments using the minimum Hypergeometric (mHG) test for differential RNA expression with aging in mouse, rat, human and African turquoise killifish samples using KEGG 2017 gene sets. The mouse data are a subset of the panel shown in **Supplemental Fig. S4G** and are plotted as a reference point. (B) DESeq2 normalized $\log_2$ fold change per unit of time during aging for genes orthologous to differentially expressed mouse genes in this study in rat and human (GTEx) samples, combining male and female samples. The p-values reported were calculated using a one sample one-sided Wilcoxon test, to test the differences between observed fold changes and 0 (*i.e.* no change with age). (C-D Limma-normalized $\log_2$ fold change per unit of time during aging for genes orthologous to differentially expressed mouse genes in this study in human samples (GSE61260) only in males (C) or in combined male and female samples (D) after inclusion of metabolic parameters as covariates (*i.e.* BMI and liver disease status) in 'limma', the R package used for microarray analysis. The p-values were calculated using one sample one-sided Wilcoxon test, to test the differences between observed fold changes and 0 (*i.e.* no change with age).